

Electron dichotomy on the SrTiO₃ defect surface augmented by many-body effects

Frank Lechermann,^{1,2} Harald O. Jeschke,³ Aaram J. Kim,³ Steffen Backes,³ and Roser Valentí³

¹*I. Institut für Theoretische Physik, Universität Hamburg, D-20355 Hamburg, Germany*

²*Institut für Keramische Hochleistungswerkstoffe,
Technische Universität Hamburg-Harburg, D-21073 Hamburg, Germany*

³*Institut für Theoretische Physik, Goethe-Universität Frankfurt,
Max-von-Laue-Str. 1, 60438 Frankfurt am Main, Germany*

In a common paradigm, the electronic structure of condensed matter is divided into weakly and strongly correlated compounds. While conventional band theory usually works well for the former class, many-body effects are essential for the latter. Materials like the familiar SrTiO₃ compound that bridge or even abandon this characterization scheme are highly interesting. Here it is shown by means of combining density functional theory with dynamical-mean field theory that oxygen vacancies on the STO (001) surface give rise to a dichotomy of weakly-correlated t_{2g} low-energy quasiparticles and localized 'in-gap' states of dominant e_g character with subtle correlation signature. We furthermore touch base with recent experimental work and study the surface instability towards magnetic order.

The SrTiO₃ (STO) compound has long been known for its paraelectric [1], semiconducting [2] and superconducting properties [3]. Renewed interest is fostered by the findings of a conducting two-dimensional electron system (2DES) on the STO surface [4, 5], of intricate magnetic response [6], as well as due to its intriguing role as a prominent building block in novel oxide heterostructures ([7, 8], see e.g. [9, 10] reviews). In this respect, several experiments [4, 5, 11–13] point towards the importance of oxygen vacancies for the plethora of physics emerging from the inconspicuous bulk band insulator.

Stoichiometric strontium titanate is rather unsuceptible to electronic correlations due to nominal Ti⁴⁺(3d⁰) valence. However, doping transforms STO into a material with potential for salient signatures of correlation effects. Usually the competition between electron localization and itinerancy in materials can be traced back to the interacting many-body system *at stoichiometry*. In doped STO, in contrast, defects have to build up the general correlated electronic structure from localized states affecting the low-energy quasiparticle (QP) nature beyond a conventional Anderson-model perspective.

The orbital character, filling, correlation strength and mobility of the key electronic states in doped STO is of main interest. In principle, electron doping as introduced by oxygen vacancies could fill the empty Ti-3d(t_{2g}) states at low energy. However creating an oxygen vacancy (OV) breaks the bond between Ti-3d(e_g) and O-2p. It has been shown [14–21] that as a result also 3d(e_g) spectral weight appears just below the Fermi level ε_F of the established metallic state. Investigations based on density functional theory (DFT) identify this e_g weight as associated with an 'in-gap' level due to the vacancy-induced crystal-field lowering. Depending on the local structural deformation, Ti charging, vacancy concentration and energy distance to ε_F , that spectral feature may also be interpreted as a small polaron. The latter is here defined by the localization of one electron at an isolated Ti site, i.e. forming

Ti³⁺, with sizable distortion of the surrounding oxygen octahedron and binding energy $\sim -1\text{eV}$ [22]. Recent DFT+ Hubbard U calculations for the TiO₂ rutile and anatase surface reveal that local Coulomb interactions are relevant for small-polaron formation [23].

The STO surface is readily made accessible to the creation of OVs, e.g. via in-situ crystal fracture [4] or by exposure to UV light [5]. Furthermore (angle-resolved) photoemission spectroscopy (ARPES) is ideally suited to probe the surface electronic structure. It reveals t_{2g} -like low-energy bands and a prominent high-energy peak at -1.3eV [5, 12, 13]. While the t_{2g} -band dispersion is well described in DFT-based methods [20, 21, 24], the characterization of the high-energy feature is more intriguing. Depending on the computational setup, the in-gap e_g weight from DFT+ U [20, 21] matches with the corresponding experimental peak position below ε_F . Though Kohn-Sham theory with static Hubbard- U correlations provides relevant insight [20, 21], so far a clear-cut many-body study of the interplay between high- and low-energy electron states on the oxygen-deficient STO surface has been missing. Also in a small-polaron picture the (orbital-dependent) role of electronic correlations, especially beyond static modelings, remains open.

In this work, we employ a combination of DFT with dynamical mean-field theory (DMFT) to investigate the role of correlations due to isolated oxygen-vacancy defects on the STO (001) surface. We find that many-body effects within charge self-consistent DFT+DMFT reveal novel features of the high-energy -1.3eV peak beyond the means of static correlation schemes. Localized e_g -like states with minor t_{2g} intermixing and itinerant states of exclusive t_{2g} nature with strong xy polarization coexist. An interplay of renormalized crystal fields and finite-frequency parts of the electronic self-energies drives this electronic dichotomy.

Surface defect structure. Periodic $3\times 3\times 4$ slabs model the oxygen-deficient STO (001) surface [20]. Two defect

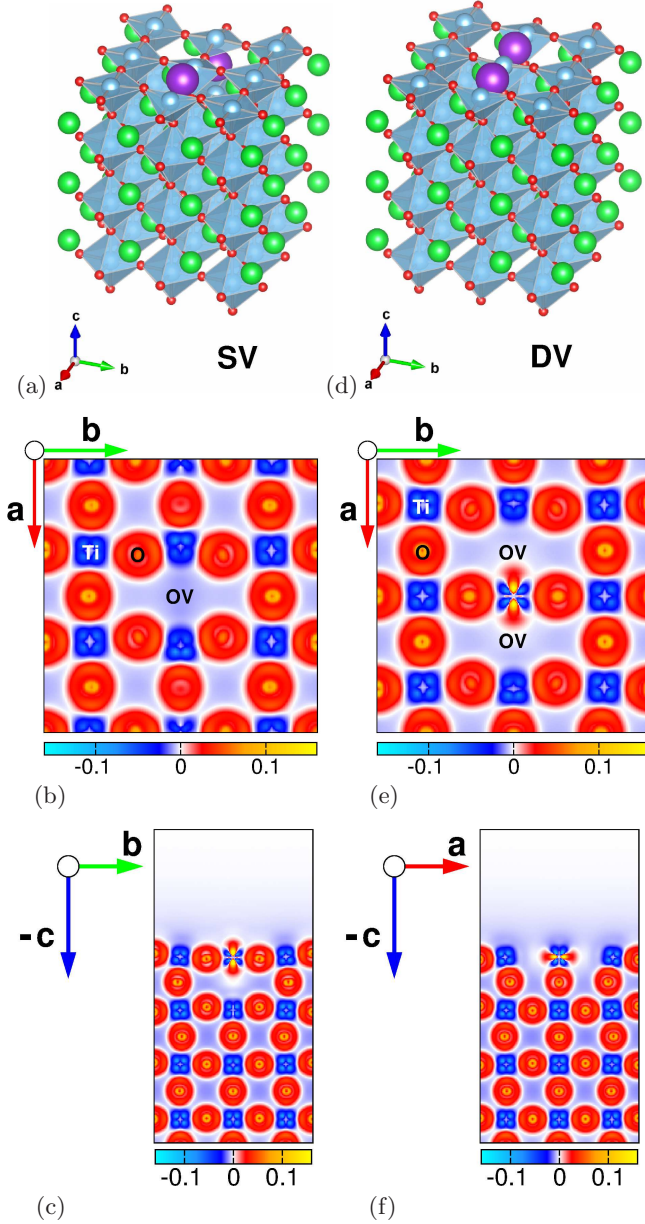


FIG. 1. (color online) DFT+DMFT bonding charge density $\rho_b \equiv \rho_{\text{slab}} - \rho_{\text{atomic}}$ for the SrTiO_3 oxygen-defect surface in the (a-c) two-single-vacancy structure (SV) and (d-f) double-vacancy structure (DV). Sr (green), Ti (lightblue), O (small red) and OV (large violet). (b,e) Top view on surface and (c,f) side view, cutting OV, respectively. The nominal $\text{Ti}^{4+}(\text{O}^{2-})$ ion loses(gains) charge compared to the free atom and thus appears blue(red).

architectures with a total of 180 atomic sites are investigated (see Fig. 1a,d). In the first single-vacancies (SV) structure there is one OV in the surface layer and the second in the SrO layer below. The second structure bears a double-vacancy (DV) defect in the surface layer, i.e., two OVs in nearest-neighbor (NN) distance (for more details see the supplementary material).

DFT+DMFT approach. A correlated subspace of three effective $3d$ orbitals on each Ti site is obtained from the projected-local-orbital formalism [25–29] (for details see the supplementary material). The Kohn-Sham problem within charge self-consistent DFT+DMFT [30–33] is addressed by a mixed-basis pseudopotential code [34], employing the generalized-gradient approximation (GGA). Continuous-time quantum Monte Carlo [35, 36] is used for the coupled single-site DMFT impurity problems. Local Coulomb interactions in Slater-Kanamori form are parametrized by a Hubbard $U=3.5\text{eV}$ and a Hund’s coupling $J_H=0.5\text{eV}$. The correlated electron problem is solved at $\beta=40\text{eV}^{-1}$.

Paramagnetic electronic structure. Two OVs amount to a vacancy concentration of $c = 0.02$ and electron-dope the slab structures with four electrons, respectively. As a general finding in line with previous work, OV-induced localized defect states are indeed of dominant e_g character. But still, both defect structures differ in their electronic characteristics, as visualized by the bonding charge density ρ_b in Fig. 1. In the SV structure, only the surface Ti site above the OV in the SrO layer below harbors an effective e_g level at lower energy. The surface-layer vacancy does not allow for such states on nearby Ti sites, but the t_{2g} levels are somewhat modified. On the other hand for the DV case, the double-OV defect only leads to effective e_g on the Ti site between the two vacancies. Hence if double-vacancy environments are available, low-energy e_g -like states are created on the embedded Ti site, also at the cost of abandoning such defect levels at Ti sites near single vacancies. Note that the subsurface oxygen vacancy in the SV case also creates such a double-vacancy scenario in an effective way, since the vacuum mimics the role of the ‘second vacancy’. Table I provides the nature and the fillings of the dominantly occupied orbitals, i.e. those forming the in-gap states. Be aware that these Ti-based φ orbitals are not of atomic but Wannier-like kind and their filling therefore includes charge from the surrounding region. The GGA crystal-field splitting between the e_g -like levels and

	$\varphi_{\text{SV}}^{(1)}$	$\varphi_{\text{SV}}^{(2)}$	$\varphi_{\text{DV}}^{(1)}$	$\varphi_{\text{DV}}^{(2,2')}$	$\varphi_{\text{DV}}^{(3)}$
GGA(PBE)	1.2	0.3	1.5	0.2	<0.1
DFT+DMFT	1.6	0.2	1.5	0.1	0.4

$$\begin{aligned}
\varphi_{\text{SV}}^{(1,2)} &\sim |z^2\rangle \quad \text{above (1) and below (2) subsurface OV,} \\
\varphi_{\text{DV}}^{(1)} &\sim -0.33|z^2\rangle + 0.94|x^2 - y^2\rangle \quad \text{on embedded site,} \\
\varphi_{\text{DV}}^{(2,2')} &\sim -0.39|z^2\rangle \pm 0.04|xz\rangle + 0.92|x^2 - y^2\rangle \quad \text{next to OVs,} \\
\varphi_{\text{DV}}^{(3)} &\sim |yz\rangle \quad \text{on embedded site,}
\end{aligned}$$

TABLE I. Wannier-like orbital states with dominant filling, centered on Ti sites. Those states form the respective in-gap states. For degenerate $\varphi_{\text{DV}}^{(2,2')}$ the electron-count sum is given.

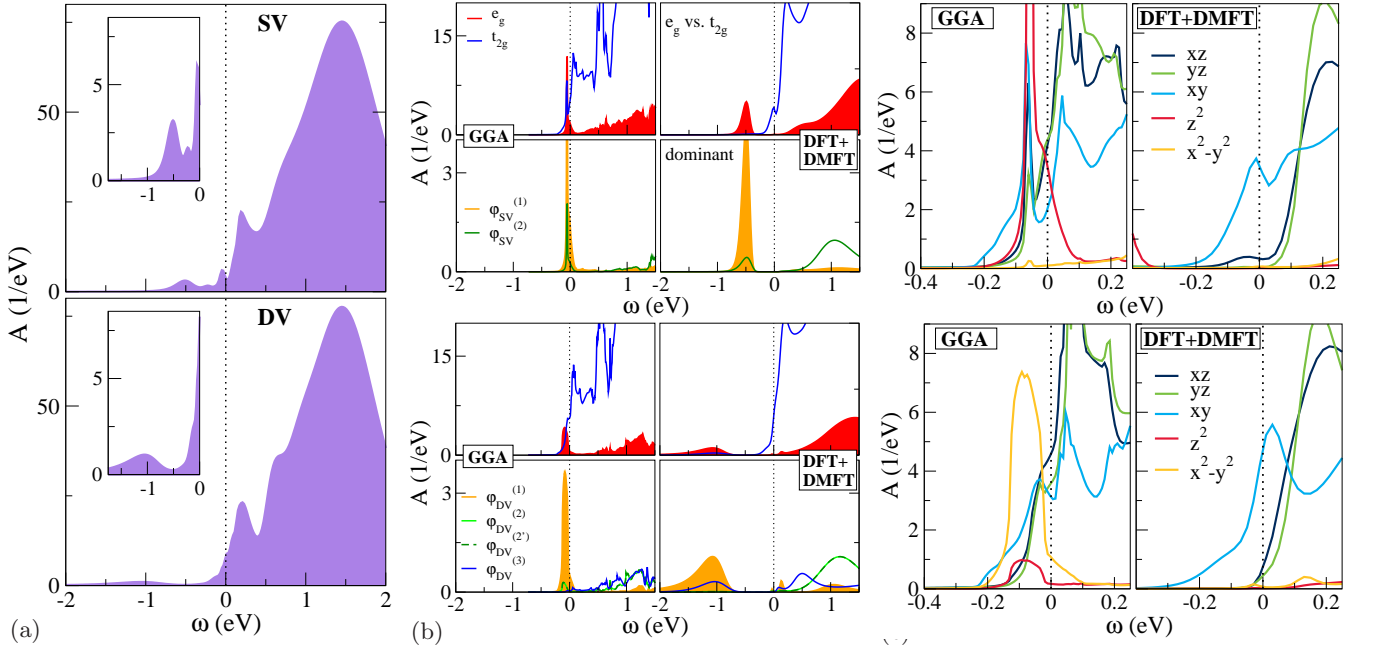


FIG. 2. (color online) Paramagnetic spectral data for SV (top row) and DV (bottom row) defect cases. (a) Total spectral function from the DFT+DMFT Bloch Green's function of the conduction states. (b) comparison with GGA concerning the e_g vs. t_{2g} occupation (top) and the dominantly occupied Ti states (bottom). (c) Low-energy Ti(3d) weight compared to GGA.

the t_{2g} states is on average on the order of 1.3 eV. Notably in DFT+DMFT, in addition to the OV-introduced e_g -like fillings, the $t_{2g}(yz)$ orbital on the embedded surface Ti ion in the DV structural case becomes localized and significantly occupied. This may be inferred from the confinement via OVs in x -direction, i.e. along the a -axis. Thus the true double-vacancy defect is effective in localizing additionally a t_{2g} state through correlations. The quasi-double-defect involving the vacuum in the SV structure is not capable thereof.

Both surfaces are metallic in GGA and DFT+DMFT. But the k -integrated spectral function with electronic correlations displays significant spectral weight transfer/shift compared to GGA (see Fig. 2b,c). The total spectral functions with correlations in Fig. 2a display for the DV case a broadened high-energy peak at -1.1 eV, i.e. close to experimental findings [5, 11–13]. A sharper peak at ~ -0.5 eV occurs for the SV structure. As shown in the local analysis of Fig. 2b, these in-gap spectral weights are mainly associated with e_g -like states already appearing on the GGA level. Electronic correlations are effective in broadening and shifting those towards higher energies. The real part of the self-energy $\Sigma(\omega + i0^+)$ renormalizes the GGA crystal field for $\omega = 0$, while the imaginary part introduces finite-lifetime effects. Note that the DV high-energy satellite has in addition sizable yz character from the embedded Ti site, whereas there is no substantial yz -orbital contribution at the associated GGA energy.

In general, standard lower-Hubbard-band interpretations are not that readily applicable. The e_g - t_{2g} hy-

bridization is weak and already small interactions shift the e_g spectral weight away from the Fermi level in the present isolated-defect cases. Furthermore, the e_g -like filling remains with and without correlations above a half-filled scenario (cf. Tab I). Both facts e.g. differ from a dense-defect limit of OVs in the $\text{LaAlO}_3/\text{SrTiO}_3$ interface, recently studied in DFT+DMFT [19]. There, a lower e_g -like Hubbard band from Ti^{3+} was identified. Here the Wannier-like $3d$ occupation centered on OV-embedded Ti in the DV structure is close to integer filling of two electrons, i.e. a local positive charging somewhat below Ti^{3+} is likely. Note that Hubbard-like signatures may indeed be attributed to the yz spectral contribution.

At the Fermi level, correlations are effective in suppressing the e_g character from GGA (cf. Fig 2b,c). Thus a clear dichotomy of only-localized and only-itinerant electrons sets in. Interestingly, for both structural cases the surface TiO_2 layer appears least conductive in DFT+DMFT. For the single-vacancy case the second transition-metal oxide layer contributes most to transport, while in the DV structure an equal share between the subsurface layers takes place. Moreover the t_{2g} -like QPs close to the Fermi level become strongly xy polarized with correlations beyond GGA. Note that due to the small doping, strong QP renormalization remains absent. The width $\Delta_{t_{2g}} \sim 0.25$ eV of this low-energy manifold agrees well with recent ARPES data [37, 38].

Ferromagnetic electronic structure. Spin-split t_{2g} -derived low-energy bands have been observed in the 2DES on the STO surface [37, 38]. Additionally, op-

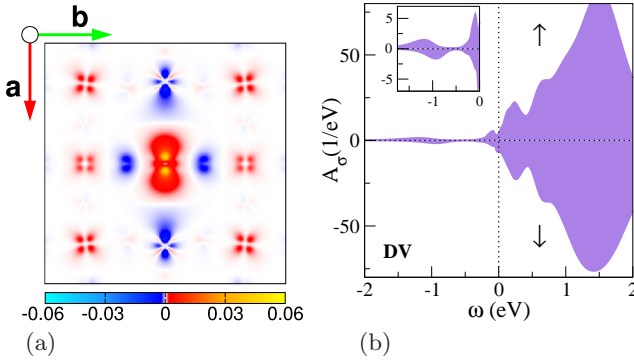


FIG. 3. (color online) Ferromagnetic DV electronic structure in DFT+DMFT. (a) Spin-resolved charge density in the ab surface plane. (b) Total Ti-based spectral function.

tically induced magnetism has been directly reported for oxygen-deficient STO [6]. In a previous DFT+U work [21] we showed that magnetism and Rashba effects compete at the doped-STO surface and that the in-gap e_g states acquire large magnetic moments. Here we study correlation effects in the ferromagnetic (FM) state beyond DFT+U [39]. When we allow for net spin polarization, the double-vacancy defect structure reveals a FM moment. No magnetic order is stabilized in the SV case. The DV magnetism is of strong local kind and spin splitting occurs mainly at the embedded Ti site (see Fig. 3a). The ordered local moment amounts to $0.22\mu_B$, whereby the $\varphi^{(1)}(\varphi^{(3)})$ orbital carries $0.14(0.08)\mu_B$. In our previous static DFT+U study for the same structure [21], larger local moments up to $0.9\mu_B$ were revealed. Thus quantum fluctuations and finite temperature are effective in reducing the ordered moment. Figure 3a shows that in the DV surface layer, the NN oxygens and the OV-adjacent Ti sites counteract the embedded moment with minor antiferromagnetic alignment.

The total spectral information in Fig. 3b displays strong spin splitting of about 0.25 eV of the satellite peak at -1.1 eV. The small yz localized-orbital contribution from the embedded Ti site is nearly exclusively spin-up polarized. In contrast to some experimental data [38] and our recent DFT+U work [21], no strong spin splitting is detected in the low-energy t_{2g} regime. This may be due to the elevated temperature, specific defect structure, or the present choice of the correlated subspace. Further work is needed to investigate this subtle issue with the ambitious DFT+DMFT framework in more detail.

Summary and discussion. Many-body and crystal-field effects induced by oxygen vacancies, here described beyond static-correlation approaches within charge self-consistent DFT+DMFT, are responsible for an apparent dichotomy in the electronic structure on the STO defect surface. Double-vacancy defects in the surface TiO_2 layer give rise to surface localized e_g dominated states as well as subsurface itinerant t_{2g} metallicity. The experimen-

tal -1.3 eV high-energy satellite is identified as an e_g -derived in-gap level that becomes broadened, shifted and dressed with minor Hubbard-band-like $t_{2g}(yz)$ weight by a frequency-dependent self-energy. Note that this localized- yz contribution may be unique to the specific architecture of the chosen DV structure. The signature of correlation is weaker in the single-vacancies defect structure, where the weakly-renormalized crystal-field character rules the nature of the in-gap state. A direct connection to oxygen vacancies in bulk STO seems difficult at first sight, since there the surface symmetry breaking is absent. But based on earlier DFT studies [14, 15] also revealing localized e_g -like states in bulk STO with such defects, the essential qualitative physics discussed here is believed to extend to the bulk regime. Moreover, in the recent DFT+DMFT study for $\text{LaAlO}_3/\text{SrTiO}_3$ [19] a similar dichotomy has been revealed.

A comment on the comparison between the DFT+U and the DFT+DMFT approach to the problem is in order. The former method treating only static correlations already provides important insight [20], also by including the Rashba physics [21]. However DFT+U mainly captures the renormalized crystal-field mechanism, fully established in that method only with symmetry breaking towards long-range magnetic order. This yields for doped STO a reasonable account of especially the integrated density of states. We here advance thereon by describing a true paramagnetic phase at finite temperature, where a competition between renormalized crystal fields and Hubbard-band-formation takes place.

The small-polaron point of view is not studied in detail, albeit structural distortions around the OV defects gives room for such an interpretation, especially in the SV case. But metallic conductivity based on low-energy quasiparticles sets in already for the present OV concentrations. Moreover, the possible deviation from a clear Ti^{3+} charge state, especially in the DV case, renders a direct small-polaron picture doubtful. Yet it cannot be excluded that polaronic transport is active in much more diluted scenarios. On the other hand, it is generally expected that a further increase of the OV concentration strengthens the Hubbard-like character of the high-energy satellite. The correlation-induced confining, here generated via the double-vacancy defect, will then be realized more effectively [19, 20]. For larger numbers of OVs the e_g - t_{2g} hybridization and -exchange will be such that e_g -like states participate in the low-energy transport [19, 40]. Further study of that crossover and inclusion of other possibly relevant ingredients such as the interplay of correlations and spin-orbit coupling beyond DFT+U or of improved non-local exchange-correlation treatments [41] are tasks for future theoretical work.

We thank G. Kresse for helpful discussions. This research was supported by the Deutsche Forschungsgemeinschaft through FOR1346. Computations were performed at the University of Hamburg and the JU-

ROPA/JURECA Cluster of the Jülich Supercomputing Centre (JSC) under project number hhh08.

-
- [1] W. Cochran, *Advances in Physics vol. 9* (edited by N. F. Mott, Taylor and Francis, Ltd., London, 1960), p. 387.
 - [2] H. P. R. Frederikse, W. R. Thurber, and W. R. Hosler, *Phys. Rev.* **134** (1964).
 - [3] J. F. Schooley, W. R. Hosler, and M. L. Cohen, *Phys. Rev. Lett.* **12**, 474 (1964).
 - [4] A. F. Santander-Syro, O. Copie, T. Kondo, F. Fortuna, S. Pailhè, R. Weht, X. G. Qiu, F. Bertran, A. Nicolaou, A. Taleb-Ibrahimi, et al., *Nature* **469**, 189 (2011).
 - [5] W. Meevasana, P. D. C. King, R. H. He, S.-K. Mo, M. Hashimoto, A. Tamai, P. Songsiriritthigul, F. Baumberger, and Z.-X. Shen, *Nat. Mat.* **10**, 114 (2011).
 - [6] W. D. Rice, P. Ambwani, M. Bombeck, J. D. Thompson, G. Haugstad, C. Leighton, and S. A. Crooker, *Nature Mat.* **13**, 481 (2014).
 - [7] A. Ohtomo, D. A. Muller, J. L. Grazul, and H. Y. Hwang, *Nature* **419**, 378 (2002).
 - [8] S. Okamoto and A. J. Millis, *Nature* **428**, 630 (2004).
 - [9] P. Zubko, S. Gariglio, M. Gabay, P. Ghosez, and J.-M. Triscone, *Annu. Rev. Condens. Matter Phys.* **2**, 141 (2011).
 - [10] H. Y. Hwang, Y. Iwasa, M. Kawasaki, B. Keimer, N. Nagaosa, and Y. Tokura, *Nature Materials* **11**, 103 (2012).
 - [11] H. Tanaka, T. Matsumoto, T. Kawai, and S. Kawai, *Jpn. J. Appl. Phys.* **32**, 1405 (1993).
 - [12] Y. Aiura, I. Hase, H. Bando, T. Yasue, T. Saitoh, and D. S. Dessau, *Surf. Sci.* **515**, 61 (2002).
 - [13] S. M. Walker, A. de la Torre, F. Y. Bruno, A. Tamai, T. K. Kim, M. Hoesch, M. Shi, M. S. Bahramy, P. C. King, and F. Baumberger, *Phys. Rev. Lett.* **113**, 177601 (2014).
 - [14] W. Luo, W. Duan, S. G. Louie, and M. L. Cohen, *Phys. Rev. B* **70**, 214109 (2004).
 - [15] Z. Hou and K. Terakura, *J. Phys. Soc. Jpn.* **79**, 114704 (2010).
 - [16] C. Mitra, C. Lin, J. Robertson, and A. A. Demkov, *Phys. Rev. B* **86**, 155105 (2012).
 - [17] N. Pavlenko, T. Kopp, E. Y. Tsybal, J. Mannhart, and G. A. Sawatzky, *Phys. Rev. B* **86**, 064431 (2012).
 - [18] C. Lin and A. A. Demkov, *Phys. Rev. Lett.* **111**, 217601 (2013).
 - [19] F. Lechermann, L. Boehnke, D. Grieger, and C. Piefke, *Phys. Rev. B* **90**, 085125 (2014).
 - [20] H. O. Jeschke, J. Shen, and R. Valentí, *New J. Phys.* **17**, 023034 (2015).
 - [21] M. Altmeyer, H. O. Jeschke, O. Hijano-Cubelos, C. Martins, F. Lechermann, K. Koepf, A. Santander-Syro, M. J. Rozenberg, R. Valentí, and M. Gabay, *arXiv:1511.08614* (2015).
 - [22] U. Diebold, *Surf. Sci. Rep.* **48**, 53 (2003).
 - [23] M. Setvin, C. Franchini, X. Hao, M. Schmid, A. Janotti, M. Kaltak, C. G. V. de Walle, G. Kresse, and U. Diebold, *Phys. Rev. Lett.* **113**, 086402 (2014).
 - [24] J. Shen, H. Lee, R. Valentí, and H. O. Jeschke, *Phys. Rev. B* **86**, 195119 (2012).
 - [25] B. Amadon, F. Lechermann, A. Georges, F. Jollet, T. O. Wehling, and A. I. Lichtenstein, *Phys. Rev. B* **77**, 205112 (2008).
 - [26] V. I. Anisimov, D. E. Kondakov, A. V. Kozhevnikov, I. A. Nekrasov, Z. V. Pchelkina, J. W. Allen, S.-K. Mo, H.-D. Kim, P. Metcalf, S. Suga, et al., *Phys. Rev. B* **71**, 125119 (2005).
 - [27] M. Aichhorn, L. Pourovskii, V. Vildosola, M. Ferrero, O. Parcollet, T. Miyake, A. Georges, and S. Biermann, *Phys. Rev. B* **80**, 085101 (2009).
 - [28] K. Haule, C.-H. Yee, and K. Kim, *Phys. Rev. B* **81**, 195107 (2010).
 - [29] M. Karolak, T. O. Wehling, F. Lechermann, and A. I. Lichtenstein, *J. Phys.: Condens. Matter* **23**, 085601 (2011).
 - [30] S. Y. Savrasov, G. Kotliar, and E. Abrahams, *Nature* **410**, 793 (2001).
 - [31] J. Minár, L. Chioncel, A. Perlov, H. Ebert, M. I. Katsnelson, and A. I. Lichtenstein, *Phys. Rev. B* **72**, 045125 (2005).
 - [32] L. V. Pourovskii, B. Amadon, S. Biermann, and A. Georges, *Phys. Rev. B* **76**, 235101 (2007).
 - [33] D. Grieger, C. Piefke, O. E. Peil, and F. Lechermann, *Phys. Rev. B* **86**, 155121 (2012).
 - [34] B. Meyer, C. Elsässer, F. Lechermann, and M. Fähnle, *FORTTRAN 90 Program for Mixed-Basis-Pseudopotential Calculations for Crystals*, Max-Planck-Institut für Metallforschung, Stuttgart (unpublished).
 - [35] P. Werner, A. Comanac, L. de' Medici, M. Troyer, and A. J. Millis, *Phys. Rev. Lett.* **97**, 076405 (2006).
 - [36] M. Ferrero and O. Parcollet, *TRIQS: a Toolbox for Research in Interacting Quantum Systems*, URL <http://ipht.cea.fr/triqs>.
 - [37] P. D. C. King, S. M. Walker, A. Tamai, A. de la Torre, T. Eknapakul, P. Buaphet, S.-K. Mo, W. Meevasana, M. S. Bahramy, and F. Baumberger, *Nat. Commun.* **5**, 3414 (2014).
 - [38] A. F. Santander-Syro, F. Fortuna, C. Bareille, T. C. Rödel, G. Landolt, N. C. Plumb, J. H. Dil, and M. Radović, *Nat. Mat.* **13**, 1085 (2014).
 - [39] Note1, our $T=290\text{K}$ in the DMFT part should be well above a reasonable magnetic-ordering temperature for rather isolated-defect induced magnetism. Due to the induced exchange splitting in the KS part, information about details of low-temperature spin ordering can still be revealed in charge self-consistent DFT+DMFT.
 - [40] M. Behrmann and F. Lechermann, *Phys. Rev. B* **92**, 125148 (2015).
 - [41] A. van Roekeghem and S. Biermann, *Europhys. Lett.* **108**, 57003 (2014).

Supplemental Information

DETAILS ON THE SURFACE STRUCTURES

For all calculations we utilize the STO experimental lattice constant $a=3.905\text{\AA}$. Periodic $3\times 3\times 4$ slabs, a vacuum-region width of $5a$ and TiO_2 termination are used to model the oxygen-deficient STO (001) surface. Two defect architectures with two vacant oxygen sites and 178 remaining atomic sites, respectively, are investigated. The SV structure has one oxygen vacancy in the surface layer and the second in the SrO layer below, with separation distance $\sqrt{17}/2a$. The DV structure has a double-vacancy defect in the surface layer, i.e., two OVs in nearest-neighbor (NN) distance a . The respective 36 Ti sites in each structural case split into 16 symmetry-inequivalent shells. Both defect-surface slabs are structurally relaxed within DFT+U [1]. While surface-layer OVs slightly repel the NN Ti ions, the subsurface vacancy attracts the Ti sites above and below.

DETAILS ON THE DFT+DMFT APPROACH

The correlated subspace within the present work is build up by three effective $3d$ orbitals on each Ti site. In order to construct this subspace in a well-defined manner we start from an initial full- $3d$ -shell five-orbital projection using $5 \times 36 = 180$ Kohn-Sham (KS) conduction states. After local orthogonalization the three most relevant projection functions are retained. Those are defined by having sizable occupation and/or weight just above ε_F , which proves reliable to reduce the number of impor-

tant local Ti projections. Due to the symmetry-lowering defect structure, the effective functions are written as linear combinations of the original cubic (e_g , t_{2g}) orbitals. Finally the three-fold projection functions on each of the 36 Ti sites yield the correlated subspace by acting on $3 \times 36 = 108$ conduction KS states. It is important to realize that the resulting real-space orbitals of the correlated subspace are not highly localized at the Ti sites, such as true atomic orbitals or the derived projection functions. This due to the minimal projection of 108 localized functions onto 108 KS states, which here also excludes explicit O-based projection functions. Hence the DMFT self-energies are associated with Wannier-like functions of some extent. An interpretation of physical observables, such as the local electron filling, in terms of atomic notions has therefore to be performed with care.

In the DFT part of the full correlated problem we use the generalized-gradient approximation (GGA) in the Perdew-Burke-Ernzerhof (PBE) form [2]. Due to symmetry, the DMFT part has to account for 16 inequivalent single-site impurity problems. In the interfacing of DFT with DMFT a double-counting correction is employed. We here put the fully-localized version [3] into practise. The complete correlated electronic structure is represented on a $4\times 4\times 1$ k -point mesh. The maximum-entropy method serves for the analytical continuation from Matsubara space to retrieve the spectral data.

- [1] H. O. Jeschke, J. Shen, and R. Valenı, New. J. Phys. **17**, 023034 (2015).
- [2] J. P. Perdew, K. Burke, and M. Ernzerhof, Phys. Rev. Lett. **77**, 3865 (1996).
- [3] V. I. Anisimov, I. V. Solovyev, M. A. Korotin, M. T. Czyzyk, and G. A. Sawatzky, Phys. Rev. B. **48**, 16929 (1993).